Thermal and Flow Analysis in a Proton Exchange Membrane Fuel Cell

Hye-Mi Jung
Graduate School, Hankuk Aviation University, Kyunggi-do 412-791, Korea
Ja-Ye Koo*
School of Aerospace and Mechanical Engineering, Hankuk Aviation University, Kyunggi-do 412-791, Korea

The effects of anode, cathode, and cooling channels for a Proton Exchange Membrane Fuel Cell (PEMFC) on flow fields have been investigated numerically. Continuous open-faced fluid flow channels formed in the surface of the bipolar plates traverse the central area of the plate surface in a plurality of passes such as a serpentine manner. The pressure distributions and velocity profiles of the hydrogen, air and water channels on bipolar plates of the PEMFC are analyzed using a two-dimensional simulation. The conservation equations of mass, momentum, and energy in the three-dimensional flow solver are modified to include electro-chemical characteristics of the fuel cell. In our three-dimensional numerical simulations, the operation of electro-chemical in Membrane Electrolyte Assembly (MEA) is assumed to be steady-state, involving multi-species. Supplied gases are consumed by chemical reaction. The distributions of oxygen and hydrogen concentration with constant humidity are calculated. The concentration of hydrogen is the highest at the center region of the active area, while the concentration of oxygen is the highest at the inlet region. The flow and thermal profiles are evaluated to determine the flow patterns of gas supplied and cooling plates for an optimal fuel cell stack design.

Key Words: PEMFC, Flow-Field, Single Cell, Pressure Distribution, Temperature Profile, Concentration Distribution

Nomenclature

A : The pre-exponential factor
$\bar{c}_p$: Mean constant pressure specific heat [J/kg·K]
$\bar{c}_p^0$: Reference constant pressure specific heat [J/kg·K]
$\bar{c}$: Mean constant volume specific heat
D_m : Molecular diffusivity [m^2/s]
e : Internal energy [W/m^2]
E_a : Activation energy for the reaction
$F_{h,j}$: Diffusional thermal energy flux in direction x_j [W/m^2]
$F_{m,j}$: Diffusional flux component in direction x_j
h : Static enthalpy [J/kg]
K_i : Porosity [m^3/m^3]
H_m : Heat of formation [J/kg]
k : Thermal conductivity [W/m·K]
m : Mass [kg]
m_m : Mass fraction of mixture constituent
$\dot{m}$: Mass flow rate [kg/s]
M : Molecular weight
n : Number of cell
P : Piezometric pressure [Pa]
P_e : Total power in the stack [Watts]
Q : Heating rate [Watts]
S_m : Mass source
S_h : Energy source
S_i : Momentum source

* Corresponding Author,
E-mail : jykoo@hau.ac.kr
TEL : +82-2-300-0116; **FAX** : +82-2-3158-2191
School of Aerospace and Mechanical Engineering, Hankuk Aviation University, Kyunggi-do 412-791, Korea. (Manuscript **Received** March 2, 2001; **Revised** September 27, 2002)

T : Temperature [K]
T_0 : Reference temperature [K]
u_i : Superficial velocity [m/s]
u_j : Absolute fluid velocity [m/s]
$\tilde{u}_j$: Relative velocity in fluid local coordinate frame [m/s]
U_a : Fraction of the air usage
U_H : Fraction of the hydrogen usage
V_c : Cell voltage [V]
x_j : Cartesian coordinate frame

Greek symbols

ρ : Density [kg/m^3]
β : Temperature exponent
β_i : Permeability
μ : Viscosity [N·s/m^2]
τ_{ij} : Viscous stress tensor [N/m^2]
ξ_j : Orthotropic direction
$\prod$: Product of all constituents
$\sum$: Summation over all mixture constituents

1. Introduction

Fuel cells are considered as the alternative devices to generate electric power in transportation and stationary applications. A schematic diagram of the Proton Exchange Membrane Fuel Cell (PEMFC) is shown in Fig. 1. Among different types of fuel cells, the PEMFC is the most promising type for transportation and small-scale electric power generation applications. PEMFC operates at lower operating temperature than the other types of fuel cells and has better electro-mechanical load characteristics.

The PEMFC stack is composed of two electrodes (anode and cathode) and a polymer electrolyte membrane. The gas channel for each electrode is shown in Fig. 2. Hydrogen and oxygen gases react to form water, electricity, and heat in a fuel cell stack. Hydrogen is supplied at the anode channel where it dissociates into charged protons and electrons. This process is given by Eq. (1). The protons diffuse through the polymer membrane, but electrons are blocked in the polymer electrolyte membrane. The electrons travel from the fuel cell anode and the anode terminal, through an electrical load, back to the cathode

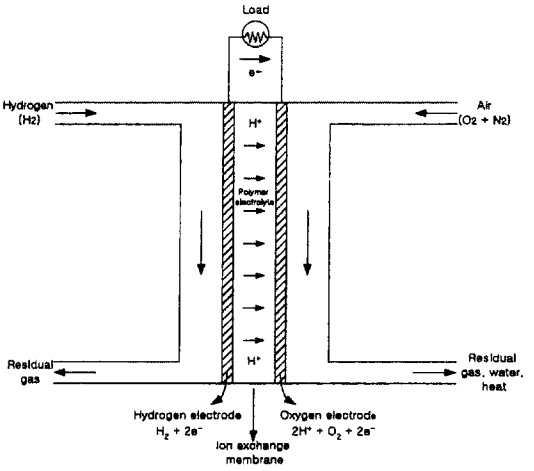

Fig. 1 Schematic of an individual fuel cell (Adopted from Fuel Cell Hand Book, 2000)

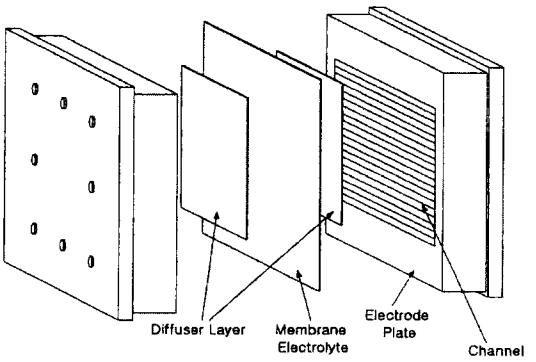

Fig. 2 Components of single PEMFC

terminal and the cathode. At the cathode, oxygen, electrons from the electrical load, and protons from the membrane combine to form water as shown in Eq. (2).

$$H_2 \rightarrow 2H^+ + 2e^- \tag{1}$$

$$\frac{1}{2} O_2 + 2e^- + 2H^+ \rightarrow H_2O \tag{2}$$

A single cell has been considered in a model. A schematic diagram of a cell is shown in Fig. 3. Three bipolar plates are provided in a single cell arrangement. The channels extend across the major surface (active area) between a feed fluid inlet and an exhaust outlet. The feed gases reach the catalyst laden Membrane Electrode Assembly (MEA) through a porous diffusion layer.

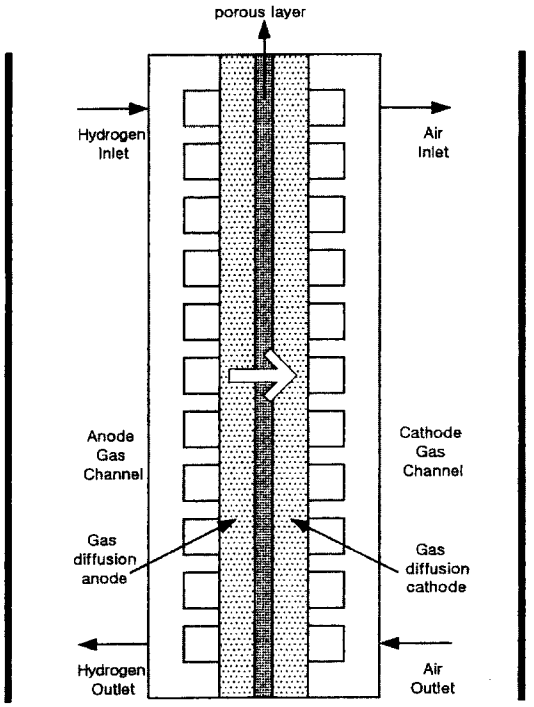

Fig. 3 Schematic diagram of a PEMFC

The phenomenon in porous diffusion layer allows a spatial distribution in the current density on the membrane in both the direction of bulk flow and the direction orthogonal to flow. The pressure distribution and temperature profile are evaluated through three-dimensional numerical simulations.

The voltage and current produced by the electrochemical reaction in the stack depend on the configuration of channels in a bipolar plate and the operating conditions such as stack temperature, and anode/cathode gas pressures. The heat generation rate at the stack is calculated as follows :

$$Q=P_e\left(\frac{1.25}{V_c}-1\right) \tag{3}$$

Better understanding and proper modeling of such processes are indispensable for improvement and optimization of the design of PEMFC systems. Because of complexity of the processes and difficulty in obtaining closed form solutions, one-dimensional isothermal conditions are assumed in most models. The models of Verbrugge and Hill (1990), Springer et al.(1991), Bernardi and Verbrugge (1992), and Fuller and Newman (1993) introduce additional equations to account for mass trasport limitations using the Stephan-Maxwell equation for gas transport. All these models have provided useful insight and reasonable predictions of the cell performance, but failed to reproduce the abrupt drop observed experimentally at higher current densities. More recently, two dimensional isothermal and non-isothermal models were presented by Standaert and Hemmes (1996) who considered heat transfer in the stack. He and Chen (1998) calculated the heat and mass transfer using the three-dimensional model. The information of concentration is obtained in this paper. These results remain applicable only to single cell with relatively simple geometry and flow channel configuration.

Today, considerable attention has been given to the computational research related to fuel cell performance analysis and optimization. Many institute and industrial companies have started to use the methods and techniques offered by computational fluid dynamics to understand and optimize electrochemical processes that take place in fuel cells. Computational analyses are capable of predicting the flow, pressure, temperature, and the current distributions in a specified fuel cell. However, most of the previous researches involving PEMFC are limited to a single channel and utilize symmetry assumptions on channel sides. It is necessary to extend the entire cell or stack to understand the practical PEMFC performance.

In this paper, the velocity, pressure, temperature, and concentration distributions are predicted for the entire single cell. A single cell with active area of 400 cm^2 is investigated numerically for performance analysis and optimal design. This analysis can be used not only to investigate flow, thermal, and concentration analysis, but also to obtain the information for design and operation of PEMFC systems.

2. Numerical Method

2.1 Numerical model

Figure 3 shows the schematic of a PEMFC.

The PEMFC can be divided into six sub-regions ; the anode gas channel on bipolar plate, the anode gas-diffusion layer, the membrane, the cathode gas-diffusion layer, the cathode gas channel on bipolar plate, and the cooling channel on bipolar plate. The configurations of the hydrogen flow channels, the air flow channels, and the cooling water flow channels are shown in Fig. 4. The PEMFC has a main channel flow paths grooved in bipolar plate as shown in Fig. 4. These plates have active area of 400 cm^2.

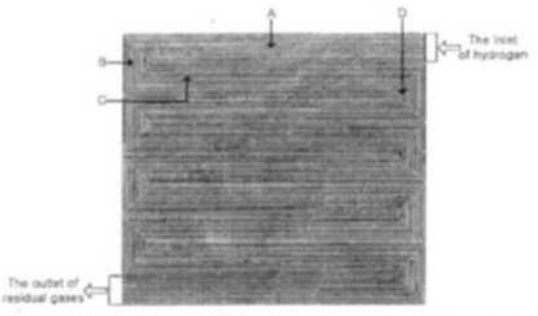

(a) The hydrogen flow chanel configuration on flow-field plate

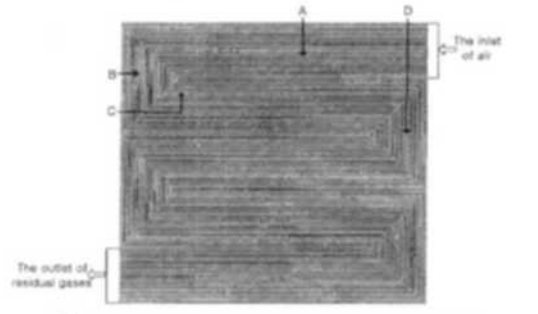

(b) The air flow channel configuration on flow-field plate

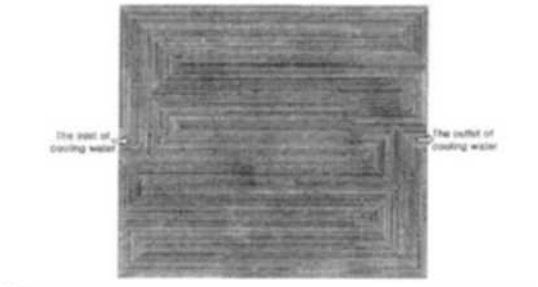

(c) The cooling water flow channel configuration on flow-field plate

Fig. 4 Flow channel configuration of flow-field plates (2-D)

For preliminary procedure for PEMFC modeling, two-dimensional model is applied to the flow-field. Since the performance of PEMFC is affected by consumption of hydrogen in the channel side, the anode and the oxygen at the air flow channels, the concentrations of hydrogen and oxygen are calculated. Three-dimensional model is applied in order to get the insight of interactions between the flow and species fields in the channel and the gas diffuser. The hydrogen from the anode flow channel is transported through the diffusion layer towards the ionomeric porous layer. The PEMFC reactor is modeled as a three-dimensional object. The processes are assumed to be a steady-state, involving multi-species. Hydrogen gas is assumed to be impermeable across the mambrane. Air in the cathode channel transports oxygen and reacts with protons.

Figure 5 shows a three-dimensional domain. The unit stack has three bipolar plates. The flow-field of hydrogen and water (cooling) has 9 serpentine passages in the flow path. The length of the hydrogen and cooling flow path is approximately 20 cm in the axial direction. The bipolar plate has 5 serpentine passages for air flow. The length of air flow path is also approximately 20 cm in the axial direction. In order to consider

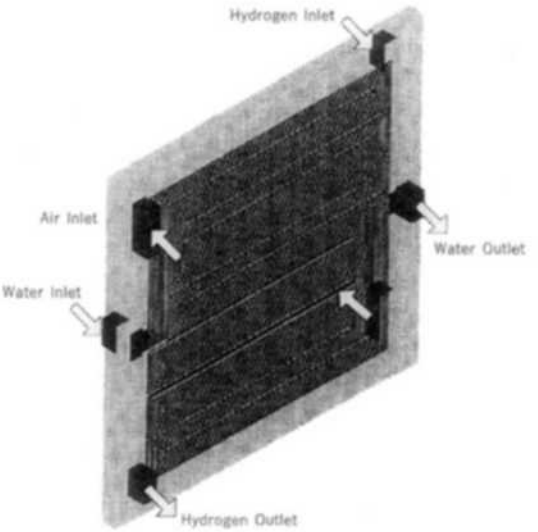

Fig. 5 Grid arrangement used in 3-D model

the influence of manifold on flow field, manifolds are included in the domain of calculation. Manifolds supply bipolar plates with gases in PEMFC. The channel flow has an effect on global flow pattern directly. The phenomenon of flow between the manifold and the channel is evaluated through a three-dimensional analysis.

The fluid flows at the channels in the anode and the cathode are the cross flows. The cross flow has advantage of evacuating the water in the cathode formed from chemical reaction. It has also advantage of jointing many fuel cell stacks. The inlet is assumed to face the outlet in the hydrogen carbon plates, and the inlet and outlet of the oxygen carbon plates are also assumed to face each other.

Since the performance of a PEMFC is affected by distributions of velocity, pressure, temperature, and concentration for a species in a single cell of the fuel cell, theses are calculated. A single cell consists of six regions ; anode, anode gas-diffusion layer, membrane, cathode gas-diffusion layer, cathode, and cooling plate. In the numerical analysis, variables are pressure, temperature, and three velocity components in the Cartesian coordinates.

The numerical work of the PEMFC needs to solve the governing equations highly coupled with several variables, and use very refined meshes for many degrees of freedom to get a reason able accuracy. Initially 3,267,040 meshes are created and locally more refined on the regions having heavy pressure gradient. The number of mesh is determined by comparison of experimental and numerical results. The calculated pressure drop is compared with the experimental one. The uniformity of flow distribution inside a channel can be checked by pressure drop. A U-tube manometer is used for measuring pressure drop. Small holes are perforated in the covering plate and connectors to the U-tube are devised to measure the pressure differences between points upstream and downstream along the channels (distance between two measuring points: 13.5 cm). The pressure drop in one channel (the nearest to the inlet) at various flow rates is shown in Fig. 6. The aspect ratio of mesh is about 0.8 and the number of mesh in the radial direction in the numerical calculation is 4. More meshes over 4 in the radial direction showed almost same results. The comparison between experimental data and numerical results is also shown in Fig. 6, which shows quite a good agreement. Same mesh aspect ratio and number of mesh are adopted in the serpentine fuel cell. The conservation equations of mass, mo-

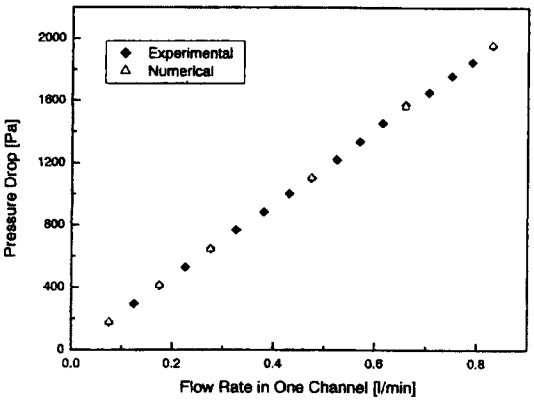

Fig. 6 Comparison between experimental and numerical straight channel pressure drops

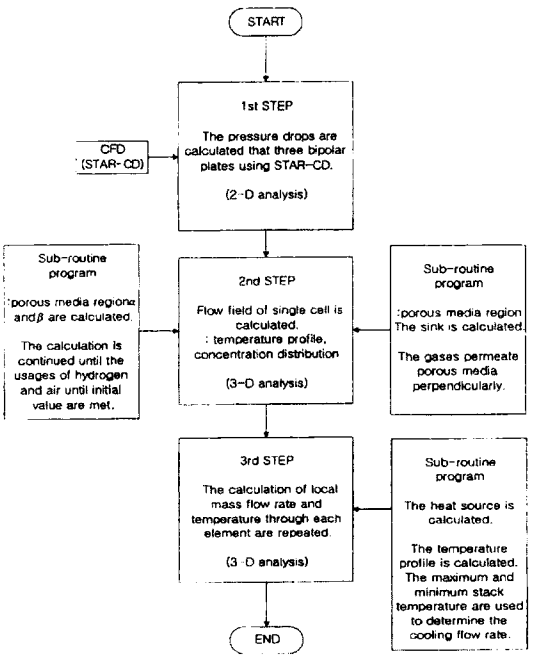

Fig. 7 Diagram of a single cell modeling numerical procedure

mentum, and energy are solved using the commercial software, STAR-CD, modified to include the electro-chemical aspects of a fuel cell. The numerical procedure is shown in Fig. 7.

2.2 Governing equations

Flows are considered either laminar or turbulent depending on regions. The flow of open channels in the bipolar plates is modeled as laminar. The Reynolds number is 1,640 in this region. The pressure gradients are small and the velocities in the open channels are also small. The flow of porous media is modeled as turbulent because the flow in a porous media is turbulent even though Reynolds number is low. This turbulent flow pattern in the porous media causes active chemical reaction (Fand, 1987).

The fuel cell operation under isothermal conditions is described by mass, momentum, energy conservation principles. The mass conservation equation is

$$\frac{\partial}{\partial x_j}(\rho \tilde{u}_j) = S_m \tag{4}$$

where $\tilde{u}_j$ is the relative velocity in fluid local coordinate frame and S_m is the mass source term. The source term should be considered in PEMFC because hydrogen and oxygen react and some of them are consumed. The mass source term can be considered as a sink and contains electro-chemical aspects of a fuel cell. More specifically, these terms correspond to consumption of hydrogen and oxygen in the electrode. In this paper, S_m is calculated using a sub-program connected to the STAR-CD. The S_m term is

$$S_{m_{anode}} = S_{H_2(g)} + S_{N_2(g)} + S_{H_2O(g)} \tag{5}$$

$$S_{m_{cathode}} = S_{O_2(g)} + S_{N_2(g)} \tag{6}$$

where $S_{H_2(g)}$, $S_{N_2(g)}$, $S_{N_2(g)}$, and $S_{H_2O(g)}$ are non-zero volumetric source terms.

For the flow through the porous media, the void volume or pore can be regarded as a distributed resistance. The gas permeability equation can be obtained from the balance between the pressure forces and the resistance forces in the porous media.

$$-K_i u_i = \frac{\partial p}{\partial \xi_i} \tag{7}$$

where ξ_i is the orthotropic direction, K_i is permeability, and u_i is the superficial velocity in direction ξ_i.

The permeability K_i is assumed to be a quasi-linear function of the superficial velocity magnitude $|\vec{v}|$.

$$K_i = \alpha_i |\vec{v}| + \beta_i \tag{8}$$

where α_i and β_i represent the permeability coefficients in porous media. The hydrogen and air permeate in the orthogonal direction. These results are shown in Fig. 8. These constant values are determined by numerical calculation.

The Darcy's law is adopted to describe the

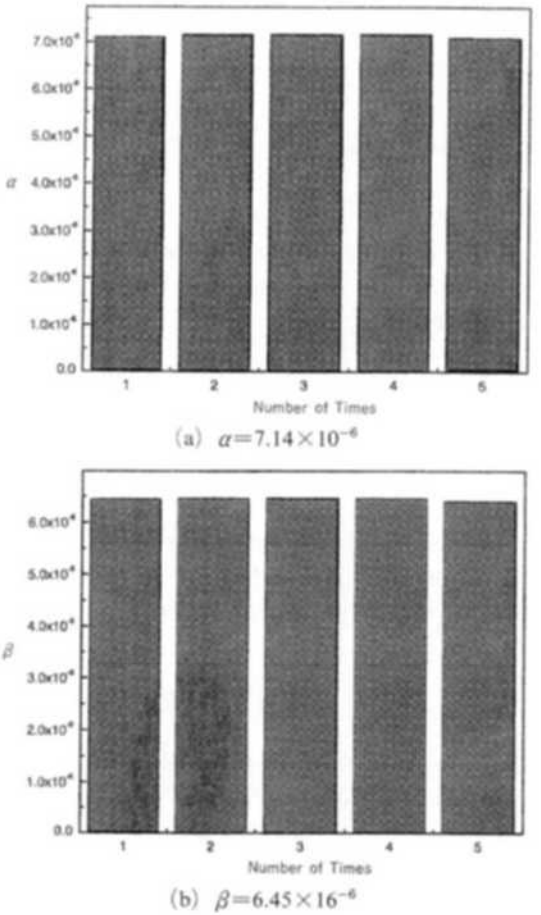

Fig. 8 The numerical experimentation of permeability determination

momentum transport in the porous media.

$$\frac{\partial}{\partial x_j}(\rho\tilde{u}_j u_i - \tau_{ij}) = -\frac{\partial P}{\partial x_i} + s_i \quad (9)$$

where τ_{ij} is the stress tensor components. This specialized equation of flow in the fuel cell involves application of ensemble or time averaging if the flow becomes turbulent. The moment source term s_i is used to describe Darcy's drag for flow through porous electrodes, active catalyst layers, and membrane. If there is very small hydraulic permeability in the membrane region, the pore velocity becomes very small. Eq. (9) containing moment source term is solved with Eq. (7) simultaneously. These terms are contributed to gas diffusion permeability in the diffusion layers. The permeability is assumed to be isotropic.

The heat transfer is implemented through the following general form of the enthalpy conservation equation for a fluid mixture.

$$\frac{\partial}{\partial x_j}(\rho\tilde{u}_j h - F_{h,j}) = \tilde{u}_j \frac{\partial P}{\partial x_j} + \tau_{ij}\frac{\partial u_i}{\partial x_j} + s_h \quad (10)$$

where h is the static enthalpy, m_m the mass fraction of mixture constituent m, H_m the heat of formation in the constituent m, and s_h is energy source.

$$h = \bar{c}_p T - c_p^0 T_0 + \sum m_m H_m = h_t + \sum m_m H_m \quad (11)$$

It should be noted that the static enthalpy is defined as the sum of the thermal and chemical components.

For solids and constant density fluids, such as water, this CFD code solves the transport equation for the specific internal energy, e, which is given as

$$e \equiv \bar{c}\,T - c^0 T_0 + \sum m_m H_m \quad (12)$$

The governing equation for total chemico-thermal enthalpy H can be obtained by summing the equations for mechanical energy conservation and the static enthalpy equation. During the calculation, it is assumed that the molecular diffusive fluxes of heat and mass obey Fourie's and Fick's laws.

$$\frac{\partial}{\partial x_j}(\rho\tilde{u}_j H - F_{h,j} - u_i\tau_{ij}) = -\frac{\partial}{\partial x_j}(u_{cj}P) + s_i u_i + s_h \quad (13)$$

$$F_{h,j} = k\frac{\partial T}{\partial x_j} + \sum_m h_m \rho D_m \frac{\partial m_m}{\partial x_j} - \bar{\rho}\overline{u_j' h'} \quad (14)$$

where k is the thermal conductivity, D_m the molecular diffusivity of constituent m, and h_m is the static enthalpy. The source term s_h can be obtained from Eq. (3).

The species transport is solved to calculate the mass flow rates. The reactant velocity of u, v, w and diffusion mass fluxes are obtained by solving the following equation.

$$\frac{\partial}{\partial x_j}(\rho\tilde{u}_j m_m - F_{m,j}) = s_m \quad (15)$$

The density is evaluated from the equation of state ;

$$\rho = \left[\sum_m \left(\frac{m_m}{\rho_m}\right)\right]^{-1} \quad (16)$$

where m_m, ρ_m and s_m are mass fraction, density, and source term of constituent m, respectively.

The overall species conservation equation is

$$\sum_m m_m = 1 \quad (17)$$

The chemical reaction rate is given as ;

$$R = -AMT^{\beta}\prod_m \left(\frac{\rho m_m}{M_m}\right)^{\upsilon m} e^{-Ea/RT} \quad (18)$$

It is necessary to solve the differential transport equations with chemical reaction for each participating reactant.

2.3 Boundary Conditions

Flow, heat, and mass transfer in the regions of distributed resistance are solved using a finite volume method. The source term in the momentum equations at the boundaries includes only resistance term of contact parts. The other convective and diffusion terms are neglected because mass transfer of hydrogen and oxygen occurs in the orthogonal direction of reactive surface. For pressure, the PISO algorithm is used. The initial values of calculation are produced using the SIMPLE algorithm. Species transport equations are solved following the bulk flow calculation. Inlet pressure for both hydrogen and

air is assumed 222,915 Pa during the two-dimensional flow-field analysis.

The three-dimensional computational domain has three inlets and three outlets. Three types of inlet boundary conditions in a gas channel are described in Table 1. The mass flow rates of hydrogen, air, and cooling water are calculated using Eqs. (19)-(21). The operating conditions are selected such that the cell voltage, V_c, is 0.65V (Lamine and Dicks, 2000).

$$\dot{m}_{air}=1.285\times\frac{1}{U_a}\times\frac{P_e}{V_c} \tag{19}$$

where P_e is the total power in the stack, V_c the voltage of each cell in the stack, and U_a is the fraction of oxygen used in any fuel cell system. The usage of hydrogen is derived in a similar way to oxygen.

$$\dot{m}_{hydrogen}=\frac{0.42}{U_H}\times\frac{P_e}{V_c} \tag{20}$$

where U_H is the fraction of usage of hydrogen.

The heat generated by a fuel cell can be calculated using Eq. (3). If $n\%$ of this heat is removed by cooling water, the mass rate of cooling water is given as follows:

$$\dot{m}_{cooling}=\frac{nP_e}{c_p\Delta T}\left(\frac{1.25}{V_c}-1\right) \tag{21}$$

where ΔT is the temperature difference between the inlet and the exit of the total fuel cell system.

Pressure and velocity distributions over the electrolyte plates can be obtained using the mass flow rates in the inlet and outlet. The velocities of hydrogen, air, and cooling water at inlet are 8.3, 12.0, and 2.0 m/s, respectively.

The chemical reaction is considered between the cathode and anode bipolar plates for the three-dimensional single fuel cell and evacuation of water is investigated in this flow analysis. The usage of hydrogen is 80% and oxygen is 40% in the calculation of chemical reaction. The usage of hydrogen means that 80% of hydrogen supplied by hydrogen inlet manifold is consumed and 20% of residual gases is discharged to hydrogen outlet manifold. Also, the usage of oxygen means that 40% of supplied oxygen is consumed by chemical reaction. Oxygen is originated from the air inlet manifold. Air is assumed to contain 79% of inert nitrogen and 21% of oxygen. The residual gases, which consist of oxygen and water vapor, are discharged to the air outlet manifold. For electrochemical analysis, a sub-routine program is used. The operating condition is 101,325 Pa and the cell temperature is constant at 353 K. The bipolar plate properties are described in Table 2 for the conjugate heat transfer. The bipolar plate is made of graphite.

Table 1 Inlet boundary conditions (P_{in}=222,915 Pa)

Inlet 1 : the anode gas channel inlet	$\dot{m}=4.511\times10^{-6}$ kg/s
Inlet 2 : the cathode gas channel inlet	$\dot{m}=2.678\times10^{-4}$ kg/s
Inlet 3 : the cooling water channel inlet	$\dot{m}=3.824\times10^{-3}$ kg/s

Table 2 Properties of bipolar plates

Constant-pressure specific heat	709 J/kg·K
Thermal conductivity	1950 W/m·K
Constant-density	2210 kg/m^3

3. Results and Discussion

The performance of a PEMFC is severely influenced by configuration of flow fields. The distribution of reactants gases on the surface of the electrode can be enhanced from the flow field in the bipolar plate. The flow field plates have many flow channels on the surface for fuel and oxidant supplies. First of all, the design of flow fields is considered in this study. The serpentine flow field configurations with active area of 400 cm^2 are proposed and discussed in this paper.

The optimization of channel configuration is not straightforward and not established well till now. In this study, the flow distribution is considered mainly. This is an essential for uniform supply of reactant gases to the electrode and the effective removal of water.

Three different flow-field plates are simulated. Current flow-field for PEMFC typically consists of grooved, serpentine flow-fields through which the gaseous reactants flow. A flow-field plate consists of reactant flow channels. Flow-channel is provided with adjacent macro-porous layer,

where layer supports thin gas diffusion backing above the catalyst layer on polymer membrane. The flow in porous layer depends on the flow-channel. The configuration, width and height of channels, has an effect on concentration distribution of reactant gases. The uniform flow and pressure drop in total active area are affected by the flow-channel. Water management is affected by the cathode flow-field. The pressure difference between the anode side and the cathode side has an influence on water flux through the membrane. Each flow-field pressure drop between supplied gases inlet and discharged residual gases are calculated.

The pressure on hydrogen plate decreases along the channel flow direction as shown in Fig. 9. As expected, the pressures are decreased with increasing distance along the channels. It is seen that the pressure drop is proportional to the flow rate. The total pressure drop in hydrogen plate is 17,763 Pa. Hydrogen is assumed to be an ideal gas. The flow rate of hydrogen is the one fifth of the flow rate of oxygen as shown in Table 1. The loss of hydrogen flow is small because the flow rate of hydrogen is less than that of oxygen. The difference of partial pressure from inlet to outlet in hydrogen flow field is less than the difference of pressure in oxygen flow field. The pressure drop is almost proportional to the channel distance as shown in Fig. 9. The pressure distribution on air plate under the same operating conditions is shown in Fig. 10. The flow rate of air is five times flow rate of hydrogen. Repeated channel configurations of parallel serpentine represent same flow-pattern over and over again. The water produced by chemical reaction is discharged into the channel in air plate. Pressure drop in the cathode is a main parameter in the management of water. It is known that appropriate pressure drop from the channel inlet to the channel outlet is 1,000~3,000 Pa at atmospheric inlet pressure for easy water discharge (Watkins et al., 1991). If the pressure drop is less than 1,000~3,000 Pa in the operating condition of 0.1 MPa, the condensed water block up the flow of gases inside channel. The non-homogeneous flow field is made because the condensed water is blocked in air fluid flow. This phenomenon is connected directly with non-homogeneous field of temperature and current density. In this situation, the performance of fuel cell is rapidly dropping. The pressure difference in Fig. 10 is 14,060 Pa. Pressure difference using the configuration of hydrogen and air channel as given in Fig. 4(a) and (b) is appropriate for good management of water.

The pressure distribution in cooling plate is shown in Fig. 11. PEMFC has low operating temperature, typically in the range between 60 and 90℃. Thermal management is required to remove the heat produced by electro-chemical reaction in order to prevent drying out of the

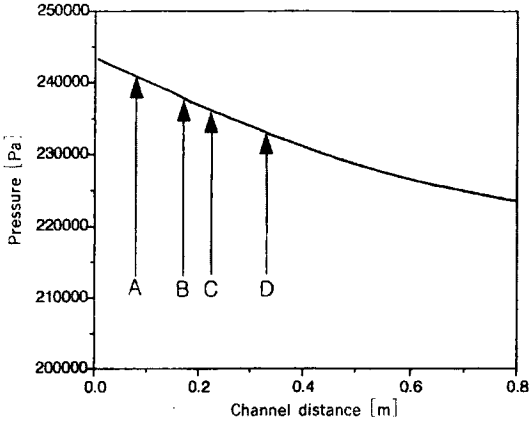

Fig. 9 The pressure distribution of hydrogen flow channel on flow-field plate

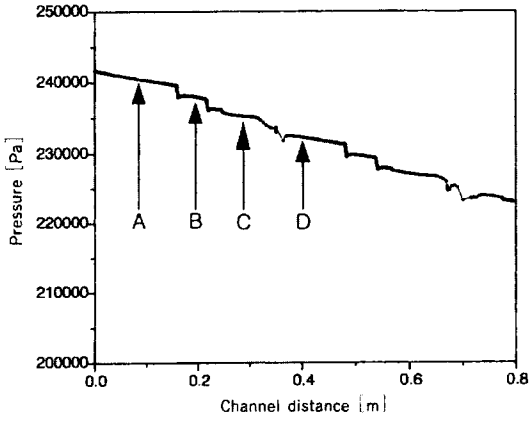

Fig. 10 The pressure distribution of air flow channel on flow-field plate

membrane and excessive operating temperature. The coolant in the channels is liquid water. The cooling water is incompressible with constant density of 998.2 kg/m^3. The pressure of cooling channel decreases linearly along the channel. The total pressure drop along the channel is about 390 Pa.

The numerical simulation is focused on mainly temperature distribution, rates of reaction of chemical species, and heat transfer for thermal management on PEMFC. It is assumed that the fuel cell is operated under steady state. The concentrations of hydrogen and oxygen become thinner along the channels as the chemical reaction occurs. In converting the hydrogen energy into electricity, the efficiency is typically about 50%. This means that a fuel cell of power x W will also have to dispose about x W of heat (Larminie and Dicks, 2000). For this reason, separate cooling plates should be added for large fuel cells. The mass flow rate of cooling water depends on the voltage and power of the fuel cell.

Figure 12 shows the contours of temperature distribution in cooling water flow-field plate. The cooling plate is inserted in each of single cell. Cooling is accomplished using water. The variation in temperature contour at two heights of the bipolar plate (solid) show small quantity of heat transfer. The temperature drop across channel of the flow-field plate is approximately 6℃. The total heating rate of a single cell is 77 W.

Figure 12 shows the temperature distribution around cooling water on flow-field. The temperature ranges of cooling water lies approximately between 77 and 80℃. This value belongs the optimum temperature distribution for heat management, which ranges between 70 and 80℃ (EG & G Services Parsons Inc., 2000). Theses results mean that the mass flow rate of cooling water calculated by Eq. (21) is adequate for heat management. This can be applied to heat management for PEMFC under another similar operating condition. The temperature profile in the section of A-A and B-B are shown in Figs. 13 and 14. The

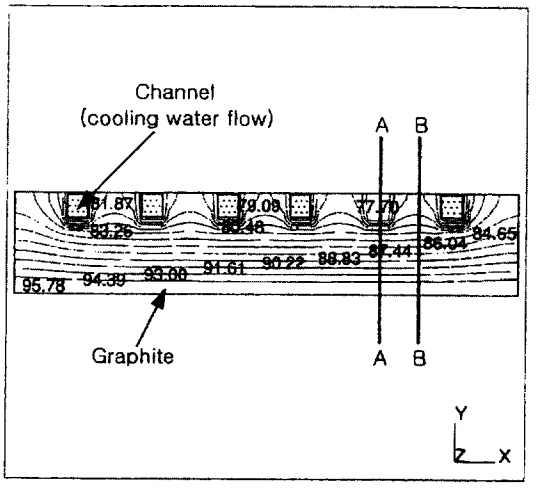

Fig. 12 Temperature distribution of cooling flow-field plate by heat transfer

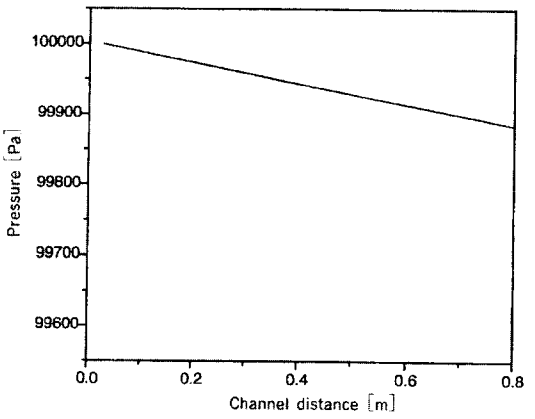

Fig. 11 The pressure distribution of cooling water flow channel on flow-field plate

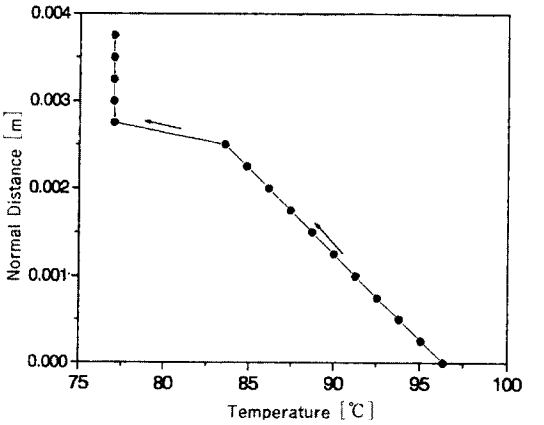

Fig. 13 Temperature distribution along normal section, A-A

temperature of cooling water is about 77 to 80℃. The temperature of the graphite decreases linearly up to 3℃. The temperature profile in the region of cooling water has changed abruptly due to discontinuity of surface.

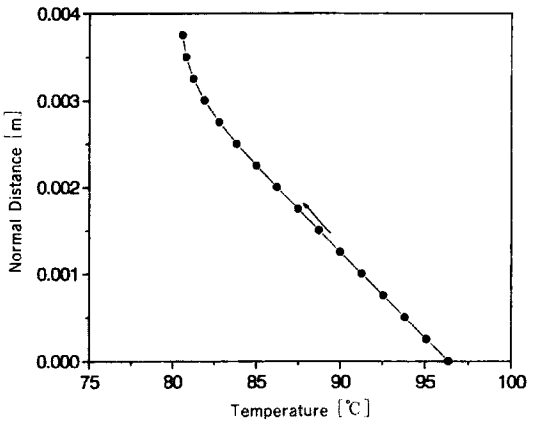

Fig. 14 Temperature distribution along normal section, B-B

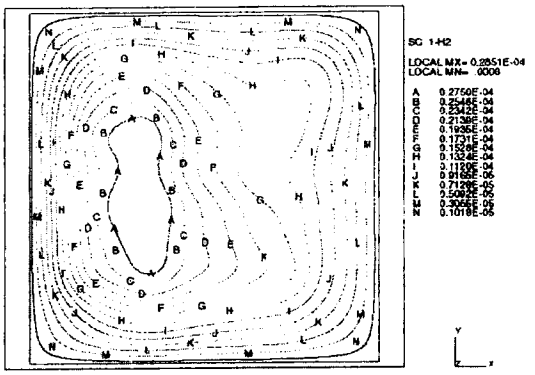

Fig. 15 Concentration pattern for hydrogen on the porous media surface of the anode side

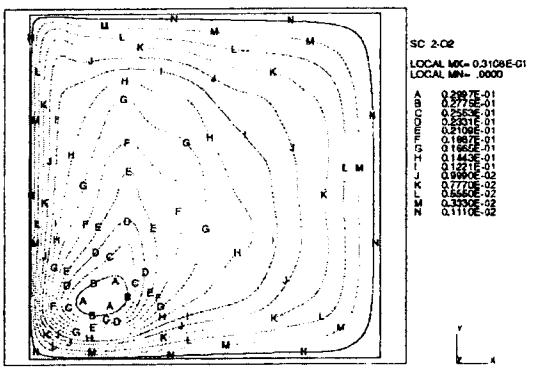

Fig. 16 Concentration pattern for oxygen on the porous media surface of the anode side

The concentrations of hydrogen and oxygen on the porous media surface are shown in Figs. 15 and 16. The anode channel consists of pure hydrogen and the cathode-side in the gas mixture consists of oxygen and nitrogen. The value of hydraulic permeability has been assumed constant through the membrane. Flows in porous media have an effect on a packed-bed chemical reactor. As a reactant is consumed at the electrode by chemical reaction, there is a loss of voltage potential due to inability of the surrounding material to maintain the initial concentration of bulk fluid. Then, a concentration gradient is formed. The transport of reactants depends on concentration. Figure 15 shows that hydrogen slowly decreases over the porous media surface during chemical reaction process. The hydrogen is consumed up to a pre-determined fraction, where the usage of hydrogen, U_{H_2}, is 0.8. Rarified hydrogen gas is supplied to the anode inlet. Hydrogen gas is considered as an ideal gas due to its low molecular weight. The distribution in the porous media at the mid-section in Fig. 15 is concentric and its fast diffusive movement causes high concentration at the center. Figure 16 shows the oxygen concentration contours of the oxygen consumption rate when the usage of air, U_{air}, is 0.4. Air is supplied though the inlet of the cathode bipolar. Air is mainly composed of nitrogen and oxygen. The cathode-side gas mixture consists of 79% nitrogen and 21% oxygen. Nitrogen concentration is then obtained by the following Eq. (22).

$$x_{N_2} = 1 - x_{O_2} - x_{H_2O} \tag{22}$$

The information of oxygen concentration is useful for prediction of the performance in PEMFC (Lee and Lalk, 1998). The concentration of oxygen depends on the nature of reactants, pressure, and temperature. The results are mainly associated with chemical kinetics and turbulence intensity. The concentration of oxygen becomes the highest in the inlet region and decreases in the outlet region as shown in Fig. 16. Even though

there are some gradients in the concentration of the hydrogen and oxygen, the maximum difference is 3.7% at the edge of the plate.

4. Conclusion

A numerical analysis for a PEMFC has been performed considering chemical reaction and turbulent effect. The flow field plates such as hydrogen, air, and cooling plate are grooved serpentine channels. The channel flow in the electrolyte plates was considered as the turbulent flow to include the diffusivity in the porous media using a three-dimensional flow analysis.

(1) The pressure drops on hydrogen and air bipolar plates channels of parallel serpentine type are approximately 17,763 Pa and 14,060 Pa at the inlet pressure boundary condition of 202,650 Pa. The suggested configuration of parallel serpentine channel type is appropriate because the total pressure drop is 10% and the rate of pressure drop is uniform throughout the channels.

(2) The distribution of temperature around the cooling water flow-field plate ranges between 77 and 80℃. The suggested configurations of parallel serpentine channel type with the suggested mass flow rate of cooling water, operating pressure, the usage of gases are appropriate for heat management of total PEMFC stack.

(3) The distribution of hydrogen in the porous media concentric and its fast diffusive movement causes high concentration at the center. The concentration of oxygen is the highest at the inlet region and decreases at the outlet region. Even though there are some gradients in the concentration of hydrogen and oxygen, the maximum difference is 3.7% at the edge of the plate.

References

Baschuk, J. J. and Li Xianguo, 2000, "Modeling of Polymer Electrolyte Membrane Fuel Cells with Variable Degrees of Water Flooding," *J. Power Sources*, Vol. 86, Issues 1-2, pp. 181~196.

Bernardi, D. M. and Verbrugge, M. W., 1992, "A Mathematical Model of a Solid Polymer Electrolyte Fuel Cell," *J. Electrochem Soc.*, Vol. 139, No. 9, pp. 2477~2491.

Costamagna, P., 2001, "Transport Phenomena in Polymeric Membrane Fuel Cells," *Chem. Eng. Sci.*, Vol. 56, Issue 2, pp. 323~332.

Dutta, S., Shimpalee, S. and Van Zee, J. W., 2001, "Numerical Prediction of Mass-Exchange Between Cathode and Anode Channels in a PEM Fuel Cell," *J. Heat and Mass Transfer*, Vol. 44, Issue 2, pp. 2029~2042.

EG & G Services Parsons Inc., 2000, *Fuel Cell Handbook*, No. DE-AM26-99FT40575.

Fand, R. M., Kim, B. Y. K., Lam, A. C. C. and Phan, R. T., 1987, "Resistance to the Flow of Fluid through Simple and Complex Porous Media Whose Matrices are Composed of Randomly Packed Spheres," *ASME J. Fluids Engineering*, Vol. 109, pp. 268~274.

Fuller, T. F. and Newman, J., 1993, "Water and Thermal Management in Solid Polymer Electrolyte Fuel Cells," *J. Electrochem Soc.*, Vol. 140, No. 5, pp. 1218~1225.

Gunes, M. B., 2001, "Investigation of a Fuel Cell Based Total Energy System for Residential Application," M. S. Mechanical Eng., Virginia Poly-technique Institute of University.

He, W. and Chen, Q., 1998, "Three-Dimensional Simulation of a Molten Carbonate Fuel Cell Stack under Transient Conditions," *J. of Power Sources*, Vol. 55, Issue 1, pp. 25~32.

Jung, S. Y. and Nguyen, T. V., 1998, "An Along-the-Channel Model for Proton Exchange Membrane Fuel Cells," *J. Electrochem. Soc.*, Vol. 145, pp. 1149~1159.

Larminie, J. and Dicks, A., 2000, *Fuel Cell Systems Explained*, John Wiley & Sons, Inc.

Lee, J. H. and Lalk, T. R., 1998, "Modeling Fuel Cell Stack Systems," *J. Power Sources*, Vol. 73, Issue 2, pp. 229~241.

Mann, R. F., 2000, "Development and Application of a Generalized Steady-State Electrochemical Model for a PEM Fuel Cell," *J. Power Sources*, Vol. 86, Issues 1-2, pp. 173~180.

Nguyen, T. V. and White, R. E., 1993, "A Water and Heat Management Model for Proton-Exchange Membrane Fuel Cells," *J. Electrochem. Soc.*, Vol. 140, No. 8, pp. 2178~2186.

Raznjevic, K., 1995, *Handbook of Thermodynamic Tables*, Begell House, Inc.

Singh, D., Lu, D. M. and Djilali, N., 1999, "A Two-Dimensional Analysis of Mass Transport in Proton Exchange Membrane Fuel Cell," *J. Eng. Soc.*, Vol. 37, pp. 431~452.

Springer, T. E., Zawodzinski, T. A. and Gottesfeld, S., 1991, "Polymer Electrolyte Fuel Cell Model," *J. Electrochem Soc.*, Vol. 138, No. 8, pp. 2334~2342.

Standaert, F., Hemmes, K. and Woudstra, N., 1996, "Analytical Fuel Cell Modeling," *J. of Power Sources*, Vol. 63, Issue 2, pp. 221~234.

Suares. G. E. and Hoo, K. A., 2000, "Parameter Estimation of a Proton-Exchange Membrane Fuel Cell Using Voltage-Current Data," *Chem. Eng. Soc.*, Vol. 55, pp. 2237~2247.

Tuomas Mennola, 2000, "Design and Experiment Characterization of Polymer Electrolyte Membrane Fuel Cells," *Master's Thesis*, Department of Engineering Physics and Mathematics, Helsinki University of Technology.

Um, S. K., Wang, C. Y. and Chen, K. S., 2000, "Computational Fluid Dynamics Modeling of Proton Exchange Membrane Fuel Cells," *J. Electrochem. Soc.*, Vol. 147, No. 12, pp. 4485~4493.

Verbrugge, M. W. and Hill, R. F., 1990, "Transport Phenomena in Perfluorosulfonic Acid Membrane during the Passage of Current," *J. Electrochem Soc.*, Vol. 137, pp. 1131~1138.

Wang, Z. H., Wang, C. Y. and Chen, K. S., 2001, "Two-Phase Flow and Transport in the Air Cathode of Proton Exchange Membrane Fuel Cells," *J. Power Sources*, Vol. 94, Issue 1, pp. 1~11.